Nuclear Inst. and Methods in Physics Research, A 1026 (2022) 166195

Contents lists available at ScienceDirect

Nuclear Inst. and Methods in Physics Research, A

journal homepage: www.elsevier.com/locate/nima

A fast-timing array of 2" x 2" $LaBr_3$:Ce detectors for lifetime measurements of excited nuclear states

L. Msebi [a,b,*], V.W. Ingeberg [c], P. Jones [b], J.F. Sharpey-Schafer [f], A.A. Avaa [b,e], T.D. Bucher [a], C.P. Brits [b,d], M.V. Chisapi [b,d], D.J.C. Kenfack [b,d], E.A. Lawrie [b], K.L. Malatji [b,d], B. Maqabuka [a,b], L. Makhathini [b], S.P. Noncolela [a,b], J. Ndayishimye [b], A. Netshiya [b], O. Shrinda [g], M. Wiedeking [b,e], B.R. Zikhali [a,b]

[a] University of Western Cape, Physics Department, P/B X17, Bellville, ZA7535, South Africa
[b] Department of Subatomic Physics, iThemba Laboratory for Accelerator Based Sciences, P.O Box 722, Somerset West, ZA-7129, South Africa
[c] Department of Physics, University of Oslo, N-0316, Oslo, Norway
[d] Physics Department, Stellenbosch University, P/B X1, Matieland, 7602, South Africa
[e] School of Physics, University of the Witwatersrand, 1 Jan Smuts Avenue, Braamfontein, Johannesburg, 2000, South Africa
[f] Department of Physics, University of Zululand, Private Bag X1001, KwaDlangezwa, 3886, South Africa
[g] Sol Plaatje University, Department of Physical and Earth Sciences, Private Bag X5008, Kimberley 8301, South Africa

ARTICLE INFO

Keywords:
Lanthinum Bromide
Lifetime measurements
Digital pulse processing
Slope method
Centroid shift method

ABSTRACT

With its unique combination of excellent timing properties and good energy resolution, $LaBr_3$:Ce detectors have proven to be effective tool in gamma spectroscopy and in particular fast-timing studies. Eight 2" x 2" $LaBr_3$:Ce detectors used in conjunction with the 16 channel all-digital waveform 500 MHz acquisition module, PIXIE-16 were commissioned at iThemba Laboratory for Accelerator Based Sciences, South Africa. The results presented here give insight of the performance of the 2" x 2" $LaBr_3$ detectors when used in conjunction with a digital pulse processing (DPP) module and electronic read-out module. Initial commissioning experiments were done using radioactive sources, including ^{60}Co, ^{152}Eu and ^{67}Ga. The detectors were then exposed to an in-beam environment using the AFRODITE array with targets ^{45}Sc and ^{64}Ni, with a proton beam energy of 27 MeV.

1. Introduction

In the study of nuclear spectroscopy, it is desirable to detect gamma rays with high efficiency, good energy resolution, as well as to study decay properties of excited states with very short lifetimes. Previously there were limitations obtaining full energy peak events while benefiting from excellent timing resolution. This was as a consequence that scintillator detectors are traditionally known to have poor energy resolution. The advent of $LaBr_3$:Ce detectors has made it possible to achieve excellent timing resolution and good energy resolution with easy maintenance. Often, these detectors are used with the conventional analogue acquisition system. The present work makes use of these detectors together with high speed digital readout electronics. Digital pulse processing (DPP) modules boast of on-board processing as well as the ability to detect pulse pileup, energy filtering, record time stamps, coincidence triggering, and perform pulse shape analysis.

Excited states in a crystal scintillator decay by emission of scintillation light which directly influences the timing resolution. The short decay time of these detectors also means that they are not susceptible to deadtime when exposed to high count rates. $LaBr_3$:Ce detectors have a very high light output of around 61×10^3 photons per MeV [1], which is significantly larger when compared to that of the NaI scintillator (38×10^3 ph/MeV [2]). Because the light output is proportional to the energy absorbed and provides better statistics and signal-to-noise ratio, it makes the high light output beneficial for energy resolution. The $LaBr_3$:Ce is an inorganic crystal with an hexagonal (UCL3 type) structure with a P63/m space group [3]. The crystals are cerium Ce^{3+} doped thus producing luminescence in the blue/UV part of the electromagnetic spectrum (λ max = 380 nm) [4]. The crystal shape optimizes the solid angle thus improving light collection and time resolution. $LaBr_3$:Ce detectors vary in dimensions with the commonly used ranging from 1" x 1" to 3.5" x 8". Choosing the optimal crystal size is often challenging since a delicate balance has to be reached between the intrinsic time resolution and the detector efficiency. The intrinsic time resolution weakens with the increasing crystal size whereas the converse is true for detector efficiency.

The measurement of lifetimes of excited nuclear states gives one of the most important information in determining the structure of an

* Corresponding author at: University of Western Cape, Physics Department, P/B X17, Bellville, ZA7535, South Africa.
E-mail address: msebi@tlabs.ac.za (L. Msebi).

https://doi.org/10.1016/j.nima.2021.166195
Received 25 July 2021; Received in revised form 19 November 2021; Accepted 29 November 2021
Available online 17 December 2021
0168-9002/

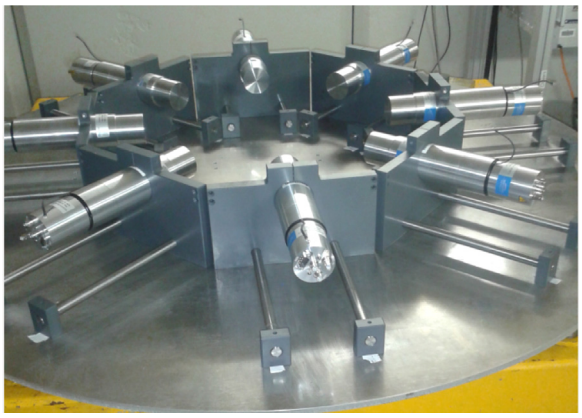

Fig. 1. The new array commissioned recently at iThemba LABS consisting of eight 2" x 2" $LaBr_3$:Ce detectors.

isotope and testing nuclear models. The lifetime of a state, together with its decay branching ratios, gives a direct measurement of the nuclear matrix elements joining an initial state to the final state. The advantage of direct electronic measurements of lifetimes is that they can be very accurate and free of many systematic errors that affect other measurements. When coupled to a gamma-ray spectrometer array such as the AFRODITE array [5], a hybrid array with capabilities of excellent energy and time resolution is obtained. These arrays are effective in measuring sub-nanosecond lifetimes, using γ-γ coincidences, over a wide range of energies [6–12]. We present here results obtained from measuring radioactive sources with 2" x 2" $LaBr_3$:Ce detectors and those obtained from in-beam measurements obtained by incorporating these detectors to the AFRODITE array.

2. Radioactive sources measurements

To test the performance of the recently commissioned eight 2" x 2" $LaBr_3$:Ce detectors, several measurements were performed with various sources. The 2" x 2" $LaBr_3$:Ce detectors with Brilliance:Ce-380 crystals were manufactured by Saint-Gobain Crystals coupled to a R2083 photomultiplier tube (PMT). The number 380 indicate the mean value of the wavelength of the emitted scintillation light [4,13]. There are two output signals from the PMT of the 2" x 2" $LaBr_3$:Ce detectors. The first is the timing signal also referred to as the fast channel stemming from the anode pulse. The second is the energy signal or the channel from the dynode pulse. The source to detector geometry was such that the point source is placed 240 mm equidistant from each detector as shown in Fig. 1. These measurements give an insight into the performance of detectors and what are the possible limitations.

The electronics of the detectors are such that they are digital and not analogue. The DPP module is connected to the 500 MHz card.

2.1. Detector electronics set up

The incoming signals are digitized and three digital filters are applied, namely; a digital constant fraction (CFD) filter, a fast and a slow trapezoidal filter. The Constant Fraction Discriminator (CFD) provides a timing signal which is related to the time of occurrence of the gamma-ray detection. The CFD algorithm, implemented in the signal processing field programmable gate array (FPGA), is unique for 500 MHz. This is because the ADC data arriving into the FPGA is initially delayed and the FPGA then locates the CFD trigger point between two adjacent 2 ns ADC samples via the weighing method. The following equation describes how the CFD algorithm is implemented [14]:

$$CFD(k) = w.\left(\sum_{i=k}^{k+L} a(i) - \sum_{i=k-B}^{k-B+L} a(i)\right) - \left(\sum_{i=k-D}^{k-D+L} a(i) - \sum_{i=k-D-B}^{k-D-B+L} a(i)\right) \quad (1)$$

Table 1
Typical parameters used for the slow and fast signal that were adjusted to achieve the best energy resolution. These values may vary slightly from detector to detector.

Parameter	Slow signal (μs)	Fast signal (μs)
Fast Risetime	0.10	0.02
Fast Flat Top	0.10	0.01
Energy Risetime	0.50	0.20
Energy Flat Top	0.50	0.10
Peak sample	0.98	0.24
Peak separation	1.00	0.50
Decay constant	34.93	0.03
CFD Delay	0.01	0.01

where $a(i)$ is the ADC trace data, k is the index representing the ADC tick (2 ns). The parameters w, B, D and L are set as $w = 1$, $B = 5$, $D = 5$ and $L = 1$.

The CFD delay and fraction are thus fixed to optimize its response. The zero crossing point is found by first building sums of ADC samples and then calculating the difference between delayed and non-delayed sums. The FPGA implements pulse detection, triggering, discrimination, pileup inspection and a trapezoidal energy filter digitally. Waveforms of each event may be customized by user defined functions such as trigger threshold, filter rise and flat top time, etc. The Digital Signal Processor (DSP) processes validated events and those events that are not validated are eliminated with zero dead time. The DSP reads out the energy filter from the FPGA and computes the pulse height and performs other tasks such as constant fraction timing and rise time calculation. It communicates with the host computer via an interface through the direct memory access (DMA) channel. A more thorough and detailed procedure is available in Ref. [15]. The DSP,s on board memory allows it to increment and store spectra. The data is collected using the iThemba LABS Digital Data Acquisition System [16].

Since the DPP module used has sixteen channels, the first eight were allocated the slow signal while the last eight were allocated the fast signal. To explore and optimize the performance of the $LaBr_3$:Ce detectors incorporated to the DPP module several radioactive sources were used.

2.2. Energy resolution and efficiency

The resolution at energy E is a ratio of the full width at half-maximum (FWHM) and the full energy peak (FEP).

The user defined functions mentioned in Section 2.1 were optimized so as to achieve the best possible energy resolution, with the typical values shown in Table 1. Parameters such as the energy risetime have a direct bearing on the energy resolution and need to be adjusted so as to produce the optimum energy resolution. Fig. 2 shows the singles spectrum of ^{60}Co radioactive source generated from one of the $LaBr_3$:Ce detectors.

The well known 1173 keV and 1332 keV peaks, from the ^{60}Co decay, can been identified together with the 1436 keV peak, from ^{138}La, that is the result of the internal radioactivity of the $LaBr_3$:Ce detector and the 1460 keV peak from presence of ^{40}K is visible. The energy resolution value obtained for the detectors is between 4.2% and 5.3% at 662 keV. It is not known exactly why the energy resolution is poorer than what is expected, as several factors may be responsible including noise induced by electronics. Test measurements are ongoing to improve the energy resolution, which include optimizing the operational voltage, since the less than expected energy resolution may also be due to a lowly optimized operational voltage. Furthermore, $LaBr_3$:Ce detectors are known to have a 2.1% energy resolution at 1332 keV [17].

The total peak efficiency of the array of eight 2" x 2" $LaBr_3$:Ce detectors was found to be $0.28\% \pm 0.0013$ at 1332 keV with the same geometry as described above.

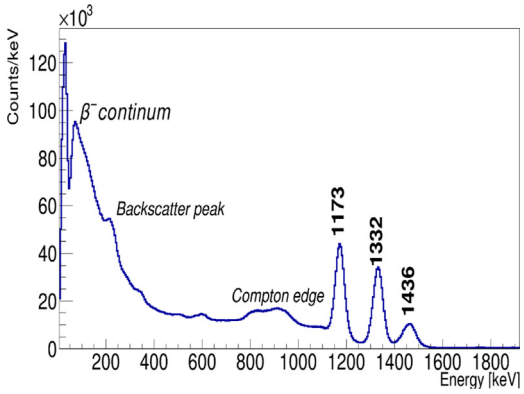

Fig. 2. The ^{60}Co singles spectrum obtained from one of the 2" x 2" $LaBr_3$:Ce detectors. The peak at 1436 keV, from ^{138}La, is due to the internal radioactivity of the $LaBr_3$:Ce detector.

Table 2
Table of the measured coincidence resolving time (CRT) obtained by varying the detector pairs in order to determine the contribution from each detector.

Detector	CRT [ps]
A11019	383.3(2.7)
A11020	318.3(3.4)
A11021	328.9(3.1)
A11022	364.1(2.8)
A11023	378.5(3.0)
A11024	379.7(3.0)
A11025	412.4(2.6)
A11026	407.9(2.6)

2.3. Time resolution

The limit of lifetimes that can be measured directly by $LaBr_3$:Ce detectors is determined by the time resolution of the detectors. To obtain the time resolution of a single detector, coincidence timing measurements of detector pairs were used for the prompt 1172–1332 keV cascade from the ^{60}Co decay. The timing resolution for the individual detectors ranged between 320 ps FWHM and 409 ps FWHM. The time resolution of the array was also measured by measuring positron annihilation γ-rays from a ^{22}Na source and gating on the 511 keV peak in the pair of detectors along the same axis. The coincidence resolving time (CRT), reported in Table 2, is extracted from the width peak for each pair.

Statistical amplitude variations affect the CFD time jitter rather than noise induced by electronics [18]. The threshold voltage, delayed time and zero crossing are CFD parameters that can be easily adjusted to produce a reliable and trustworthy results. The threshold prevents triggering from the noise by ignoring signals below the said threshold. Other factors that affect time resolution include detector size and operational voltage. A more detailed discussion may be found in [19].

3. Lifetimes of radioactive sources

Using the fast-timing technique, the transition that populates an excited state may be designated as the *start* and the one that depopulates it, may be designated *stop*. It is paramount that the energies are well resolved to clearly distinguish the transitions populating or depopulating an excited state. The quality of the measurement depends on this important ability.

The ^{67}Ga source was produced at iThemba LABS, it has a half-life of 3.26 days, decays through 100% electron capture to ^{67}Zn.

In this decay process, the 184.6 keV level decays to the ground state via the $(3/2^-) \rightarrow (5/2^-)$ transition. In this work, the lifetime of the $(3/2^-)$ state at 184.6 keV level was measured. This was obtained by measuring the time difference between two signals of the $LaBr_3$:Ce detectors. The first signal which defines the *start*, is given by the 209 keV gamma ray populating the level and the second signal, which is the *stop*, by the 184.6 keV gamma ray depopulating it.

The time spectrum obtained is shown in Fig. 3(a) through which the lifetime of the $(3/2^-) \rightarrow (5/2^-)$ transition was calculated. The slope method was employed to obtain the lifetime of this transition and other transitions that have much longer lifetimes than the system's time resolution. In this method no background subtraction was applied, since the time contribution of the background usually affects the prompt distribution. By taking a fit far from the prompt region, the background time component can be avoided. The lifetime of this transition was calculated to be $T_{1/2}$ = 1.090(7) ns. Lieder et al. [21] states this half-life to be $T_{1/2}$ = 1.01(5) ns. While Engel et al. [22] asserts it to be $T_{1/2}$ = 1.026(14) ns.

The current analysis studied the ^{152}Eu radioactive source, decays by 72.08% to ^{152}Sm via electron capture. The half-life of the first excited state (2^+) of ^{152}Sm has a reported value of 1.403(11) ns [20]. Setting the *start* and *stop* gates on transitions that populate and depopulate the 2^+ state we found the half-life to be $T_{1/2}$ = 1.394(9) ns. Various measurements, see Table 3, were performed to determine the half-life of the first excited state 2^+ of ^{152}Sm. The adopted value in the ENSDF evaluated data sheet is $T_{1/2}$ = 1.403(11) ns.

Table 3
Table of values for the half-life of the first excited state 2^+ of ^{152}Sm from previous publications.

Author and reference	Half-life (ns)
M. Birk *et al.* [23].	1.45(6)
D. Ashery *et al.* [24]	1.41(6)
P. J. Wolfe and R. P. Scharenberg [25]	1.46(5)
F. W. Richter *et al.* [26] .	1.44(3)
A. Hubner [27]	1.43(4)
W. Karle *et al* [28]	1.398(6)
C. C. Dey *et al* [29]	11.40(2)
M. R. El-Asser *et al* [30].	1.35(5)
H. W. Kugel *et al.*[31]	1.41(4)
R. E. McAdams and E. N. Hatch [32]	1.36(6)
D. B. Fossan and B. Herskind [33]	1.37(4)
A. W. Sunyar [34]	1.40(10)
M. Hellstrom *et al* [35].	1.471(35)
Present work	**1.394 (9)**
M. J. Martin [36]	1.403(11)

Another radioactive source studied in this work is ^{133}Ba, it decays to ^{133}Cs through 100% electron capture and has a half-life of 10.551 years. The $(5/2^+)$ state of ^{133}Cs is adopted as $T_{1/2}$ = 6.283(14) ns according to the ENSDF evaluated data sheet. To obtain the lifetime of this state, two detectors were used with a gate set on the 356 keV transition that populates the state and the 81 keV that depopulates it. The present work reports the half-life of this state to be $T_{1/2}$ = 6.217(12) ns (Table 4).

3.1. Time walk characteristics

Essential to obtaining accurate lifetimes of excited nuclear states is the ability to employ a walk-free signal. The inherent variation in the delay of the discriminator results in time walk and may affect the quality of the signal. For scintillator detectors, it is not good practice to ignore the time walk as it may lead to adverse effects on the time resolution of a fast-timing array. Various methods may be used to correct for the time walk of a detector [6,54–56], to optimize the input signal. In a real γ-γ fast-timing set-up, the detector dependent time-walk difference is visible although it may be compensated in the CFD. Applying a higher PMT operation voltage can reduce the time-walk non-linearity yet this can drive the energy response of the PMT into non-linearity [57].

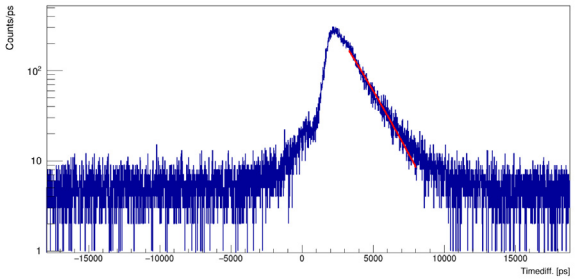

(a)

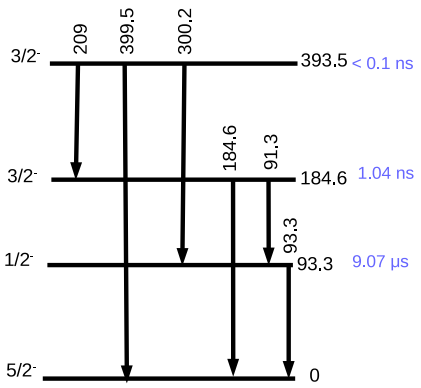

(b)

Fig. 3. (a) The time difference spectrum between two detectors fitted with exponential fit to determine the half-life of the 184.6.6 keV level of ^{67}Zn populated through the decay of the ^{67}Ga radioactive source. INSERT: The time spectrum on logarithmic scale. (b) The partial level scheme of ^{67}Zn showing the 209 keV transition populating the 184.6.6 keV level [20].

Table 4
List of published values of the half-life for the first excited state in ^{133}Cs.

Author and reference	Half-life (ns)
H. Mach *et al.* [37].	6.321(35)
E. Bodenstedt *et al.* [38]	6.31(5)
W. Flauger and H. Schneider [39]	6.30(15)
D. Bloess *et al* [40] .	6.25(5)
B. Olsen and L. Bostrom [41]	6.16(7)
F. W. Richter and J. Schutt [42]	6.25(5)
F. A. Akilov *et al* [43]	6.30(7)
A. Sakata *et al* [44] .	6.26(17)
K. G. Valivaara *et al.* [45]	6.27(4)
P.D. Bond *et al* [46]	6.28(14)
D.K. Gupta and G.N. Rao [47]	6.36(3)
D. Mouchel and H.H. Hansen [48]	6.23(3)
R. L. Graham and R. E. Bell [49]	6.0(4)
P. Thieberger [50]	6.25(10)
J.S. Geiger *et al* [51]	6.3(3)
I.M. Govil *et al* [52]	6.08(4)
D. Bloess and F. Munnich [40]	6.25(5)
Present work	**6.217(12)**
Yu. Khazov *et al* [53]	6.283(14)

For sub-nanosecond fast-timing measurements, it is necessary to establish the dependence of the time response as a function of energy. Moreover, when measuring lifetimes in the sub-nanosecond range, the centroid shift method may be employed. Characteristics of the energy as a function of the centroid position's prompt time distribution describes the time walk characteristics. The interplay of the shape of the detector output pulse and the timing principle result in the prompt response function [57].

A ^{60}Co radioactive source was used in this work to investigate the effects of the time walk. Fig. 4(a) illustrates that time walk characteristics when the *start* detector is gated on the 1173 keV and 334 keV. In order to obtain the centroid position over a wide range, 10 keV wide gates, in increments of 20 keV, were gated on the *stop* detector. The 1173 keV transition populates the 1332 keV level in ^{60}Ni following the β-decay ^{60}Co radioactive source. For comparison, a gate is set on the 344 keV Compton background as well and is an essential reference energy describing the prompt response function as elaborated by Régis et al. [58]. Similarly, gating the *stop* detector 1173 keV and 334 keV the fits as represented in Fig. 4(b) were obtained.

Below 300 keV a delayed structure, which may be a result of Compton scattered events, is observed. The 1173 keV gated centroids show an invariable continuity up to about 1200 keV and from then a structure is visible, possibly emanating from Compton scattered events.

N. Marginean et al. [6] used a second order polynomial to correct for the time walk, resulting in an optimum time resolution. The fitted

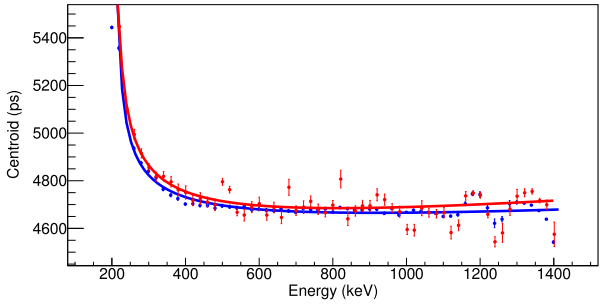

(a)

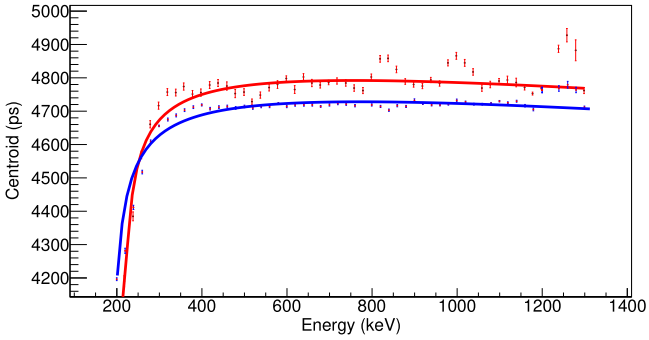

(b)

Fig. 4. (a) The energy dependency of the centroid position of the prompt time distribution obtained from gating the *start* detector on the 334 keV Compton background (in red) and 1173 keV full energy peak (in blue) transitions of the ^{60}Co source. (b) The gate is now set on the *stop* detector on the same transitions. The fitted data points in red are for gates set on the 344 keV and those in blue are for the 1173 keV.

centroids shown in Fig. 4, were fitted using:

$$C(E_\gamma) = \frac{a}{\sqrt{b + E_\gamma}} + cE_\gamma + d \tag{2}$$

4. In - beam experiment

To evaluate the performance of the 2" x 2" $LaBr_3$:Ce detectors when exposed to in-beam experimental environment, an experiment was conducted in which six 2" x 2" $LaBr_3$:Ce detectors were coupled to the AFRODITE array with eight Compton-suppressed clover detectors. Two additional large volume 3" x 8" $LaBr_3$:Ce detectors were also used.

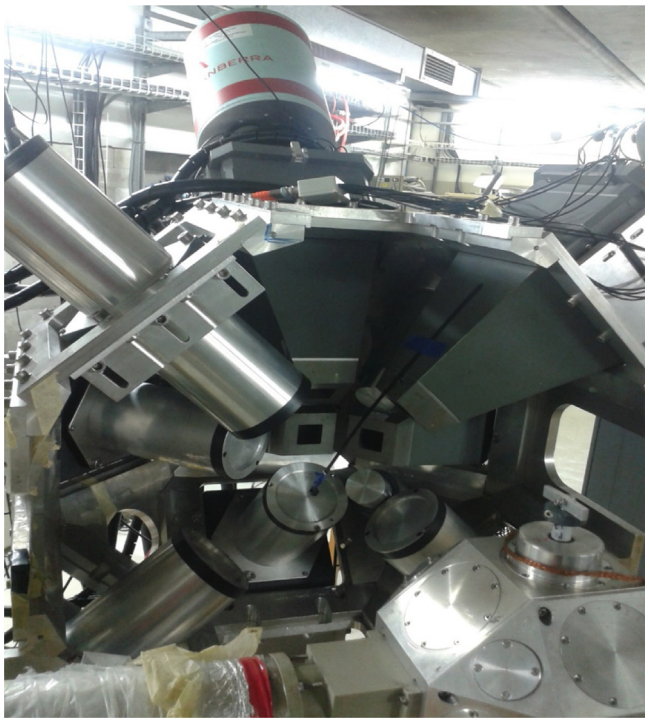

Fig. 5. The AFRODITE array consisting of HPGe clover detectors with BGO shields, large volume 3" by 8" $LaBr_3$:Ce detectors and medium sized 2" by 2" $LaBr_3$:Ce detectors.

The experimental set-up is shown in Fig. 5. High detector efficiency and excellent timing properties are obtained from large and small $LaBr_3$:Ce detectors respectively, whereas the clovers detectors offers superior energy resolution. Two of the 2" x 2" $LaBr_3$:Ce detectors were placed at an angle of 45° with respect to the beam line axis and the other four were placed at an angle 90°.

A micron semiconductor S2 type, with 48 rings and 16 sectors, was used in this work to build a particle identification telescope that consists of a thin energy loss stage in transmission geometry followed by a much thicker residual energy detector in which the particles are *stopped*. This particle dE-E telescope, used to select a desired reaction channel, was inserted inside the target chamber. The thickness of the dE detector used was 309 μm and the thickness of the E was 1041 μm. The mass and the charge of the particle both influence the energy loss per unit length.

The signals from HPGe detectors and particle telescope processed by the 100 MHz XIA digital acquisition card. In this work, results for the ^{45}Sc(p,d)^{44}Sc and ^{45}Sc(p, α)^{42}Ca reaction channels, with beam energy was 27 MeV, are reported. Two crates accommodate nuclear electronics in standard modules were used in this experiment. The first crate was fully occupied by the particle telescope and the HPGe detectors which were all incorporated into the 100 MHz XIA digital acquisition card. The second crate was used to accommodate the $LaBr_3$ detectors which were incorporated 500 MHz XIA digital acquisition card.

An arbitrary shift, between the $LaBr_3$ detector channels, in the recorded timestamp (in multiples of 2 ns in the 500 MHz card) was observed to occur whenever the DPP was restarted resulting in signals to become arbitrarily shifted in time, therefore a correction in the software was implemented. This shift is due to unsynchronized signals and in instances where DPP was left uninterrupted no shift was observed. To correct for this effect, the centroids of the time distributions were determined in order to observe how the signals were shifted during the *start* and *stop* process.

Table 5
Energy resolution $LaBr_3$:Ce detectors at 1.3 MeV obtained from the radioactive source ^{60}Co. The detector numbers recorded here are as per the label on the detectors.

Detector Number	Energy resolution at 1.3 MeV
2" x 2" $LaBr_3$:Ce 2	3.19%
2" x 2" $LaBr_3$:Ce 4	3.22%
2" x 2" $LaBr_3$:Ce 5	3.26%
2" x 2" $LaBr_3$:Ce 6	3.73%
2" x 2" $LaBr_3$:Ce 7	2.48%
2" x 2" $LaBr_3$:Ce 8	3.26%
3" x 8" $LaBr_3$:Ce 3.1	2.74%

4.1. Characterization of $LaBr_3$:Ce detectors for the in-beam set-up

The $LaBr_3$:Ce detectors were calibrated using a third order polynomial of the form:

$$E = ax^3 + bx^2 + cx + d \tag{3}$$

where a, b, c, d are the gain matching coefficients. E is the energy and x is the channel number of the original spectrum. These peaks were fitted and the relevant peak centroids and their uncertainties were taken into account so that each point has an associated weight. A correction as a result of a shift between detector channels was done [19]. The energy-independent centroids give a constant shift_{ij} values that were arranged in a matrix form, $i \times j$, for each time the data acquisition system was stopped between runs. The matrix elements $i \times j$ were arranged as 6×6 elements such that $\text{shift}_{i=j} = 0$ and $\text{shift}_{ij} = -\text{shift}_{ji}$.

The energy resolution obtained from the ^{60}Co calibration source is shown in Table 5.

Several factors influence the efficiency of detectors including the solid angle and the properties of a detector crystal. The high density and high atomic number of $LaBr_3$:Ce detectors result in higher detection efficiency. The total photopeak efficiency for the 2" x 2" $LaBr_3$:Ce detectors for the in-beam set up was obtained as $0.84\% \pm 0.0010$. The large volume 3" x 8" $LaBr_3$:Ce detectors were not the focus of this study. They are, however, part of the African $LaBr_3$:Ce Array (ALBA), at iThemba LABS, a detailed characterization of these detectors is found in Ref. [59].

4.2. The Prompt Response Difference (PRD) curve

To extract sub-nanosecond lifetimes, it is important to calibrate the zero-time response of the fast timing set-up. This involves a detailed and thorough process of determining the energy dependent centroid position of simultaneously occurring events (prompt events) of the prompt response function. Through this process, the timing characteristics describing the set-up is possible, which known as the "prompt response difference" (PRD) curve [60]. The PRD curve was determined using the ^{152}Eu radioactive source which decays to ^{152}Gd through β^- decay mode. The nucleus ^{152}Gd emits several gamma-ray transitions that are in coincidence with each other and have known picosecond lifetimes. This enables a reference energy gate to be selected and keep it constant while varying other gates that are in coincidence with the chosen reference energy gate. In this work, the 344 keV state was chosen as reference energy gate since there are seven gamma-ray transitions that are in coincidence with it. A measured centroid difference (which is the difference of the centroid position between the *start* and *stop* time distributions) is obtained which is then corrected by twice the known lifetime of the state, 2τ, to obtain each data point, which is then plotted as function of energy, yielding the PRD curve. The ^{152}Eu source also decays to ^{152}Sm through electron capture. The 244 keV transition of ^{152}Sm is populated by several transitions, and therefore is useful as a reference energy. The PRD for energy reference at 244 keV was obtained. The two PRD curves can be shifted in parallel

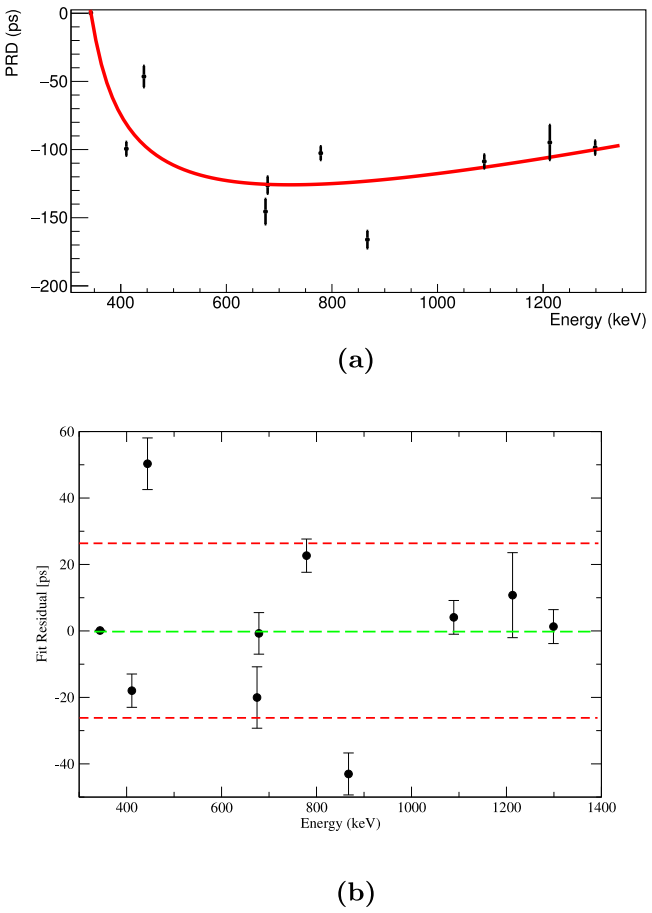

Fig. 6. (a) The PRD curve obtained after the overlapping of the two curves obtained with reference energies 344 keV and 244 keV is done. (b) The fit residual showing the data point deviation to the fit. The red dashed lines correspond to 26 ps, which is equivalent to 1σ.

so that one overlaps onto another thus making a single PRD curve see Fig. 6(a). The data points of the PRD curve are then fitted using, [60]

$$PRD(E_\gamma) = \frac{a}{\sqrt{b + E_\gamma}} + cE_\gamma + d \tag{4}$$

where a, b, c and d are free fit parameters.

No active shielding was placed around the $LaBr_3$:Ce detectors. Deviations from the smooth monotonic curve are possibly induced by Compton scattered events. Though both gates were set on full energy events to obtain the PRD curve, exposure to Compton events do contaminate the timing information of a $\gamma - \gamma$ fast-timing set-up. Compton events may result in an artificial delay in the timing information. The presence of an artificial delay in the time distributions is related to the time-of-flight of the scattered γ-ray [61].

4.3. The ^{44}Sc nucleus

The ^{44}Sc nucleus is an odd–odd nucleus with one valence proton and three valence neutrons outside the doubly magic ^{40}Ca nucleus. The ^{44}Sc nucleus has a dynamic range of excited nuclear states which makes it possible to put to test the performance of the 2" x 2" $LaBr_3$:Ce detectors.

4.3.1. The 2^- state

Instead of a $LaBr_3$:Ce detector, a reference timing signal can be synchronized with the radio-frequency (RF) of the pulsed beam to form a *start* signal and the *stop* can be provided by one of the 2" x 2" $LaBr_3$:Ce detectors. Using the RF as a reference signal has an added advantage of yielding more statistics and better results. In this work, the RF signal was used as a reference signal and also a $LaBr_3$:Ce detector as a reference signal allowing the results to be compared between RF-$LaBr_3$ and $LaBr_3$-$LaBr_3$ measurements.

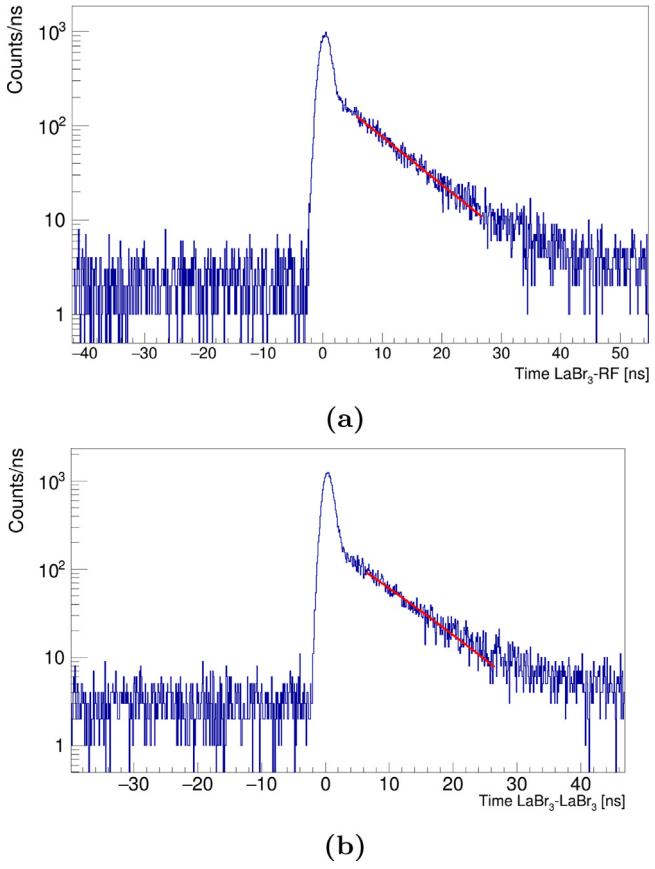

Fig. 7. (a)Time spectrum obtained by the gating the radio-frequency and a $LaBr_3$:Ce detector used to measure the half-life the 234.7 keV level. The fitted region represents events of the full energy peak. (b) Time spectrum obtained when two $LaBr_3$:Ce detectors are used, for the 234.7 keV level, in which one is a *start* and the other is *stop*.

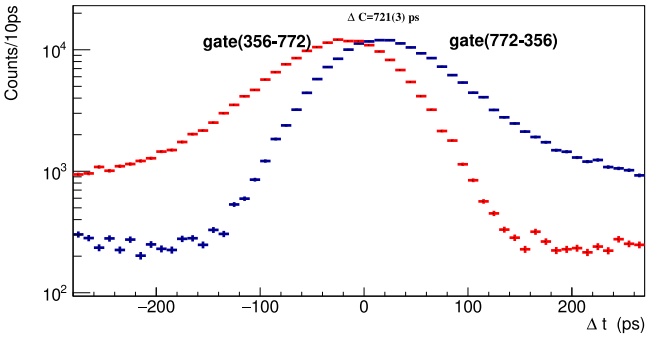

Fig. 8. Time distribution spectra for the 772 → 356 $keV\gamma$-γ cascade from which the ΔC value for the 429 keV level was obtained.

The half-life of the 234.7 keV level was measured and compared to the value reported in literature. The *start* gate was set on the feeding 396 keV, $4^- \rightarrow 2^-$, transition and a *stop* gate set on the $2^- \rightarrow 0$ transition. When the RF was used as a reference signal the lifetime obtained for the excited 2^- state, at 234.7 keV level is $T_{1/2}$ = 6.160(76) ns. The time distribution spectrum from which this half-life was measured is shown in Fig. 7(a). The half-life for the same state when using $LaBr_3$-$LaBr_3$ measurements is $T_{1/2}$ = 5.93(41) ns, with the time distribution shown in Fig. 7(b). In both time spectra two

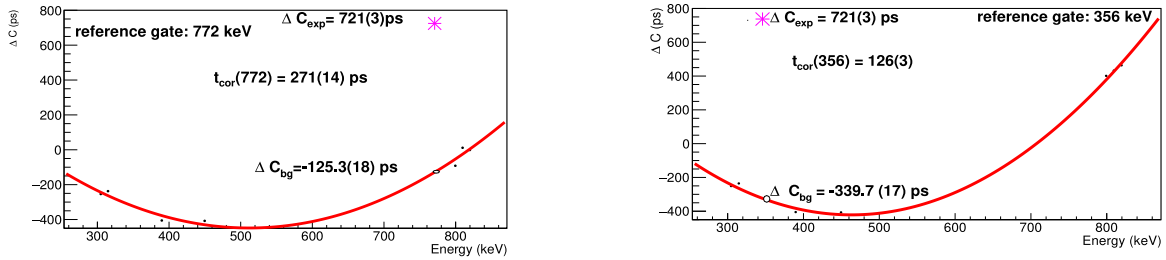

(a) (b)

Fig. 9. (a) The centroid difference as a function of energy depicting background timing-analysis with the reference gate set at 772 keV with the background gates set around the regions of FEPE at 356 keV and 772 keV. The data points are fitted using a second order polynomial. (b) The centroid difference as a function of energy depicting background timing-analysis with the reference gate set at 356 keV with the background gates set around the regions of FEPE at 356 keV and 772 keV. The data points are fitted using a second order polynomial.

components are visible; The large fast component is due to the Compton background and the slow component due to full energy peak detection. It is this slow component that the half-life of the excited 2^- state was calculated using the slope method. The value obtained in this work is $T_{1/2} = 6.160(76)$ ns while the value reported ENSDF evaluated data sheet is $T_{1/2} = 6.12(23)$ ns [20]. The results of the 2^- state at 234.7 keV level and other states of ^{44}Sc are presented in Table 6

Contributions from the large fast component may falsify lifetime measurements, however, these contributions may be avoided by fitting the slope outside the region of the Compton background. Since the background is distributed uniformly it may be determined and catered for prior the fit, which was done for the fits obtained for Figs. 7(a) and 7(b).

4.3.2. The 3^- state

By virtue of this state being a much more short lived state, in the sub-nanosecond region, the Generalized Centroid Shift Method was employed to measure the lifetime of this state and all other sub-nanosecond states. The γ-γ cascade used to measure the lifetime of this state is $5^- \rightarrow 3^-$ and $3^- \rightarrow 1^-$. The populating and depopulating gamma energies are 772.5 keV and 356.92 keV respectively.

The centroid difference value of ΔC = 721(3) ps was obtained as shown in Fig. 8 and the PRD correction factor for the combination 772.5 → 356.92 keV is given by PRD(772–356 keV) = −99(26) ps.

In this analysis to correct for the background, the Compton background correction method was employed [58]. Another background correction through analytical means has been developed by Gamba et al. [62]. In order to compute the energy-dependent centroid difference, ΔC_{bg}, gates were set around well defined background regions for both the (full energy peak events) FEPE in the (772 → 356 keV) cascade. The reference energies are the FEPE whereas the background regions are varied. Fig. 9 shows both background-timing analyses for the two experimental peak-background components fitted with a second order polynomial. The background gates were set at the same width. The $LaBr_3$:Ce and HPGe gated coincidence spectra are shown in Fig. 10. The HPGe coincidence spectrum was used to select the background gate because of its excellent energy resolution. The lifetime of the excited 3^- state is then calculated as follows, [63]:

$$\tau = \frac{\Delta C + t_{av} - PRD}{2\times} \tag{5}$$

where t_{av} is the total time correction obtained from the weighted average of two separately measured time correction terms from the feeder and the decay transitions of the $\gamma - \gamma$ cascade. The half-life of this state obtained after background correction is recorded in Table 6.

4.3.3. The 6^- state

The 6^- state at 2210.5 keV level has no known lifetime recorded in literature. In this work, the lifetime of the 6^- state at 2210.5 keV level was measured. The transition that populates this state is the $7^- \rightarrow 6^-$ and it is associated with 396.2 keV γ ray. The 2210.5 keV level is depopulated by the $6^- \rightarrow 5^-$ which is associated with the 1013 keV γ ray. The centroid difference ΔC = 316(2) ps, as illustrated by Fig. 11. The PRD correction factor for the (396 → 1013 keV) cascade is PRD(396–1013 keV) = -45(26) ps. The half-life of this state obtained after background correction, using the similar approach employed for the 3^- state, is given in Table 6.

4.3.4. The 7^- state

The 7^- state at 2606.7 keV level has no known lifetime recorded in literature. This work reports the lifetime of this state. The 2606.7 keV is populated by the 382 keV γ ray level through the $8^- \rightarrow 7^-$ transition. The depopulating γ ray is 1409 keV through the $7^- \rightarrow 5^-$ transition. The centroid difference is ΔC =344(5) ps, as illustrated by Fig. 12.

The PRD correction factor for the (382 → 1409 keV) cascade is PRD(382–1409 keV) = -33(26) ps. The half-life of this state obtained after background correction, using the similar approach employed for the 3^- state, is given in Table 6.

4.3.5. The 8^- state

The lifetime of the 8^- state at 3364.1 keV level was measured in this work and it has no known literature value. The 465 keV γ ray populates this level and it is the $9^- \rightarrow 8^-$ transition. It is also depopulated by a $8^- \rightarrow 7^-$ transition associated with the 757 keV γ ray. The centroid difference is ΔC = 292(3) ps, as illustrated by Fig. 13. The PRD correction factor for the (465 → 757 keV) cascade is PRD(465–757 keV) = -22(26) ps. The half-life of this state obtained after background correction, using the similar approach employed for the 3^- state, is given in Table 6.

4.4. The ^{42}Ca nucleus

The ^{42}Ca nucleus has only two valence neutrons outside the doubly magic ^{40}Ca nucleus. The nucleus ^{42}Ca was populated through the ^{45}Sc(p, α)^{42}Ca direct reaction.

4.4.1. The second 0^+ state

The first excited 0_2^+ state of ^{42}Ca is found at 1837.3 keV energy level and has a known half-life of $T_{1/2}$ = 387(6) ps. This state is populated by a $2^+ \rightarrow 0^+$ associated with the 587 keV gamma ray. It is depopulated by an $0^+ \rightarrow 2^+$ transition associated with the 312 keV gamma ray. Fig. 14 shows the delayed and anti-delayed time distributions from which the centroid difference was determined. The Compton background correction method was employed to correct for the background and the background-timing analyses spectra are shown in Fig. 15. The PRD correction factor for the (587 → 312) cascade is PRD(587–312 keV) = -323(26) ps. The half-life obtained for this state and other states of ^{42}Ca are compared with previous measurements in Table 7.

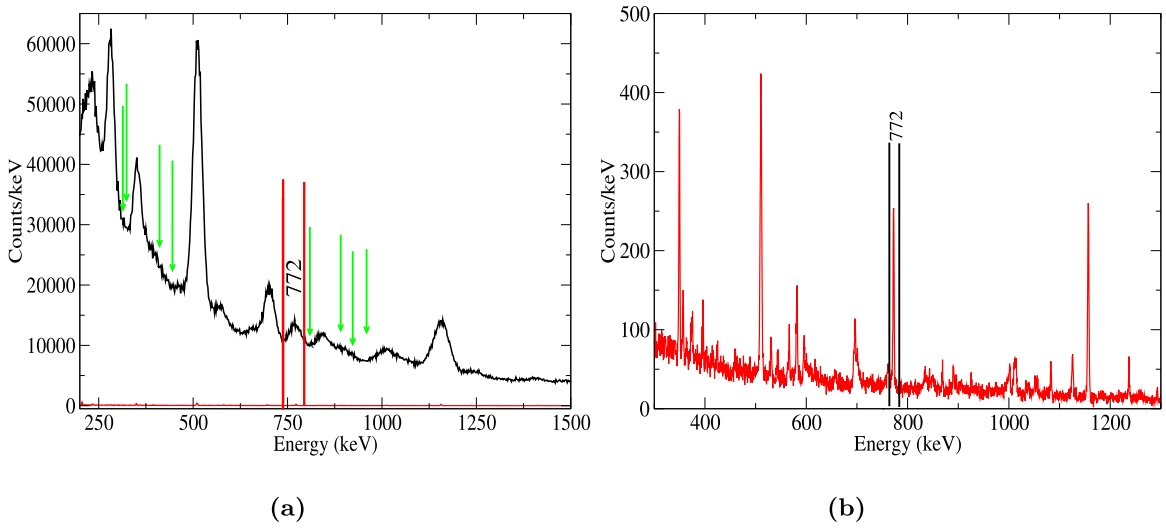

Fig. 10. (a) The γ-γ coincidence spectrum gated on the 356 keV. The full energy peak in coincidence with the 356 keV peak, used to obtain the lifetime of the excited 3^- state, is the 772 keV energy. The arrows mark the regions where the background gates around the full energy peaks were set. The black energy spectrum is the $LaBr_3$:Ce coincidence spectrum and the red energy spectrum is HPGe coincidence spectrum. (b) The HPGe gated spectrum clearly showing the 772 keV γ ray energy that is in coincidence 356 keV γ ray energy.

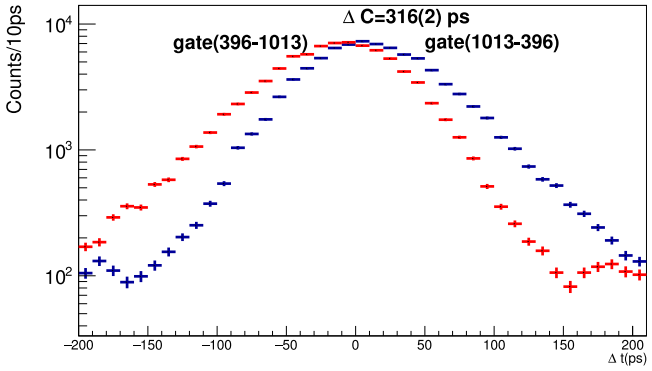

Fig. 11. Time distribution spectra for the 396 → 1013 $\gamma - \gamma$ cascade from which the ΔC value for the 2210.5 keV level was obtained.

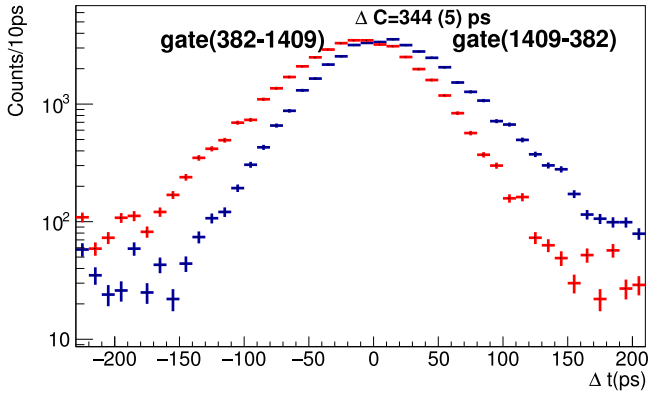

Fig. 12. Time distribution spectra for the 382 → 1409 $\gamma - \gamma$ cascade from which the ΔC value for the 2606.7 keV level was obtained.

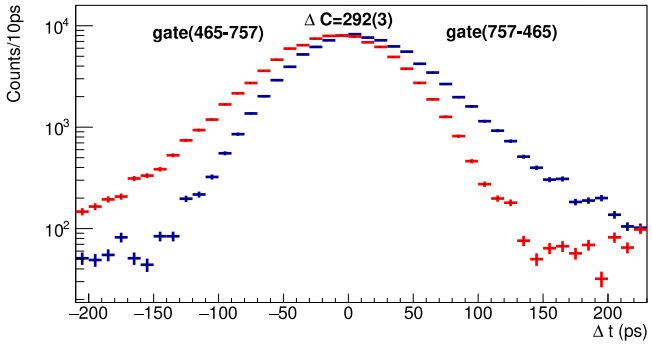

Fig. 13. Time distribution spectra for the 465 → 757 $\gamma - \gamma$ cascade from which the ΔC value for the 3364.1 keV level was obtained.

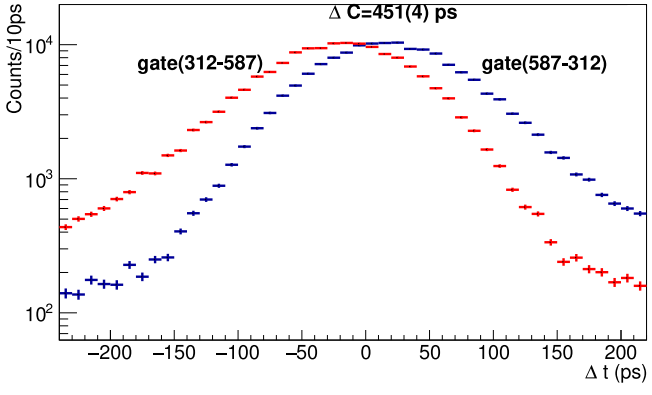

Fig. 14. Time distribution spectra for the 587 → 312 $keV\gamma$-γ cascade from which the ΔC value for the first excited 0_2^+ state of ^{42}Ca was obtained.

5. Conclusion

Eight 2" x 2" $LaBr_3$:Ce detectors used in conjunction with the 16 channel all-digital waveform 500 MHz acquisition card, PIXIE-16 were commissioned at iThemba Laboratory for Accelerator Based Sciences. Known lifetimes for ^{44}Sc and ^{42}Ca were extracted with new lifetimes for ^{44}Sc obtained. The results presented here prove that 2" x 2" $LaBr_3$:Ce detectors are a formidable tool for nuclear spectroscopy and in particular they are much useful for lifetime measurements. In this work we were able to obtain lifetimes without active shielding. Improved quality of results may be obtained in future experiments through active shielding, since this minimizes Compton background.

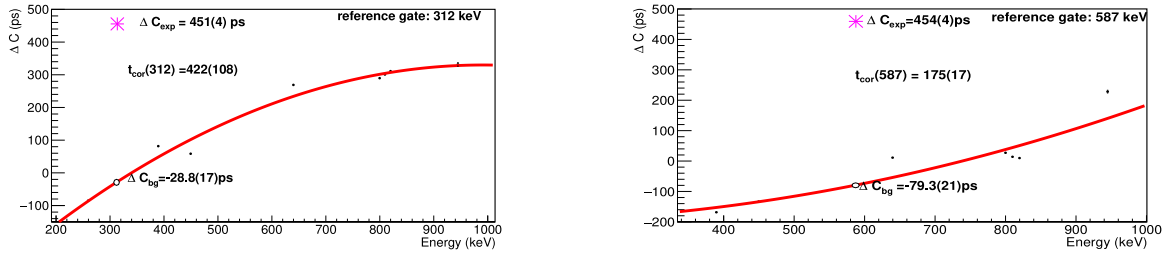

(a) (b)

Fig. 15. (a) The centroid difference as a function of energy depicting background timing-analysis with the reference gate set at 312 keV with the background gates set around the regions of FEPE at 312 keV and 587 keV. The data points are fitted using a second order polynomial. (b) The centroid difference as a function of energy depicting background timing-analysis with the reference gate set at 587 keV with the background gates set around the regions of FEPE at 312 keV and 587 keV. The data points are fitted using a second order polynomial.

Table 6
Experimentally obtained half-lives that have been published for different states of ^{44}Sc. The values obtained in the current work are highlighted in bold. The sub-nanosecond lifetimes are background corrected, via the Compton background correction are indicated by the subscript CB.

Energy level (keV)	J^π	Method	Reference	Half-life
234.7	2^-	Recoil Distance	[64]	12.7 (22)ns
234.7	2^-	Delayed coincidence	[65]	6.12 (23)ns
234.7	2^-	ENSDF Evaluation	Adopted ENSDFvalue [20]	6.12 (23)ns
234.7	2^-	Fast-Timing (RF-$LaBr_3$)	Present work	**6.160 (76)ns**
349.9	4^+	Recoil Distance	[64]	3.12 (28)ns
349.9	4^+	Recoil Distance	[66]	3.1 (3)ns
349.9	4^+	ENSDF Evaluation	Adopted ENSDFvalue [20]	3.12 (19)ns
349.9	4^+	Fast-Timing (RF-$LaBr_3$)	Present work	**3.067 (14)ns**
349.9	4^+	Fast-Timing ($LaBr_3$-$LaBr_3$)	Present work	**2.499 (15)ns**
631	4^-	Recoil Distance	[67]	381 (55)ps
631	4^-	Recoil Distance	[64]	411 (30)ps
631	4^-	ENSDF Evaluation	Adopted ENSDFvalue [20]	404 (30)ps
631	4^-	Fast-Timing (GCD_{CB})	Present work	**336 (15)ps**
428.8	3^-	Recoil Distance	[66]	380 (40)ps
428.8	3^-	Recoil Distance	[64]	378 (42)ps
428.8	3^-	ENSDF Evaluation	Adopted ENSDFvalue [20]	378 (42)ps
428.8	3^-	Fast-Timing (GCD_{CB})	Present work	**364 (10)ps**
2210.5	6^-	Fast-Timing (GCD_{CB})	Present work	**162 (9)ps**
2606.7	7^-	Fast-Timing (GCD_{CB})	Present work	**180 (10)ps**
3364.1	8^-	Fast-Timing (GCD_{CB})	Present work	**164 (12)ps**

Table 7
Experimentally obtained half-lives that have been published for different states of ^{42}Ca. The values obtained in the current work are highlighted in bold. The sub-nanosecond lifetimes are background corrected, those that are corrected via the Compton background correction are indicated by the subscript CB.

Energy level (keV)	J^π	Method	Reference	Half-life
3189.3	6^+	Doppler Shift Attenuation	[68]	5.30 (16)ns
3189.3	6^+	Delayed Coincidence Techniques	[69]	3.7 (5)ns
3189.3	6^+	Doppler Shift Attenuation	[70]	5.3 (3)ns
3189.3	6^+	Delayed Coincidence Techniques	[71]	5.52 (15)ns
3189.3	6^+	ENSDF Evaluation	Adopted ENSDFvalue [20]	5.30 (16)ns
3189.3	6^+	ENSDF Evaluation	Adopted ENSDFvalue [20]	5.30 (16)ns
3189.3	6^+	Fast-Timing (RF-$LaBr_3$)	Present work	**4.91 (4)ns**
3189.3	6^+	Fast-Timing ($LaBr_3$-$LaBr_3$)	Present work	**4.29 (5)ns**
1837.3	0^+	Direct electronic timing	[72]	387(6)ps
1837.3	0^+	Delayed Coincidence Techniques	[73]	330 (20)ps
1837.3	0^+		[74]	420 (11)ps
1837.3	0^+	ENSDF Evaluation	Adopted ENSDFvalue [20]	387(6)ps
1837.3	0+	Fast-Timing (GCD_{CB})	Present work	**391 (17)ps**

CRediT authorship contribution statement

L. Msebi: Methodology, Formal analysis, Investigation, Writing – original draft, Review and editing. **V.W. Ingeberg:** Writing – original draft, Data curation. **P. Jones:** Conceptualization, Software, Supervision, Fund acquisition. **J.F. Sharpey-Schafer:** Supervision, Visualization, Conceptualization. **E.A. Lawrie:** Writing – original draft. **M. Wiedeking:** Project administration.

Declaration of competing interest

The authors declare that they have no known competing financial interests or personal relationships that could have appeared to influence the work reported in this paper.

Acknowledgment

We would like to acknowledge financial assistance and support from the National Research Foundation (NRF), South Africa under the following grants: (99037,90741,105207)

References

[1] P. Dorenbos, et al., IEEE Trans. Nucl. Sci. NS-51 3 (2004) 1289.
[2] I. Holl, E. Lorenz, G. Magera, IEEE Trans. Nucl. Sci. 35 no. 1 (1988) 105–109.
[3] B. Morosin, et al., J. Chem. Phys. 49 (1968) 2007.
[4] C.M. Rozsa, et al., Brilliance 380 Scintillator Perforamnce Summary, 2009.
[5] J.F. Sharpey-Schafer, Nucl. Phys. News. Int. 14 (2004) 5.
[6] N. Marginean, et al., Eur. Phys. J. A 46 (2010) 329.
[7] J.M. Régis, et al., Nucl. Instrum. Methods A 726 (2013) 191.
[8] T. Alharbi, et al., Phys. Rev. C 87 (2013) 014323.
[9] T. Alharbi, et al., Appl. Radiat. Isot. 70 (2012) 1337.
[10] P.J.R. Mason, et al., Phys. Rev. C 88 (2013) 044301.
[11] S. Kisyov, et al., J. Phys. Conf. Ser. 366 (2012) 012027.
[12] S. Kisyov, et al., Phys. Rev. C 84 (2011) 014324.
[13] Scintilation Products Technical Note available at, www.detectors.saint-gobain.com.
[14] XIA LLC. CFD Algorithm for 500 MHz Pixie-16, Tech. rep., XIA LLC., Sept. 2016..
[15] XIA LLC. PIXIE-16 User's Manual. Version 3.03, 2018, URL http://www.xia.com.
[16] iThemba LABS Annual Report 2013, URL https://tlabs.ac.za/wp-content/uploads/pdf/annual_reports/Annual_Report_2013_small.pdf.
[17] D. Weisshaar, et al., Nucl. Instrum. Methods A 594 (2008) 56.
[18] H. Spieler, IEEE Trans. Nucl. Sci. NS-29/3 (1982) 1142.
[19] L. Msebi, Lifetime Measurements of Excited Nuclei Through Modern Nuclear Spectroscopy (Ph.D. thesis), University of the Western Cape, 2021, in press.
[20] National Nuclear Data Center, URL http://www.nndc.bnl.gov/nudat2/chartNuc.jsp.
[21] R.M. Lieder, et al., Nuclear Phys. A 106 (2) (1967) 389.
[22] H. Engel, et al., Naturfosch 27a (19) 1368.
[23] M. Birk, et al., Phys. Rev. 116 (1959) 730–733.
[24] D. Ashery, et al., Nucl. Phys. 77.3 (1966) 650–656.
[25] P.J. Wolfe, R.P. Scharenberg, Phys. Rev. 160 (1967) 866–873.
[26] F.W. Richter, et al., Z. Phys. 213 (1938) 202.
[27] A. Hubner, Z. Phys. 183 (1965) 25.
[28] W. Karle, et al., Nucl. Instr. Methods A 271.3 (1998) 507–511.
[29] C.C. Dey, et al., Can. J. Phys. 70 (1992) 268.
[30] M.R. El-Asser, et al., Z. Naturfosch. 27a (1972) 1229.
[31] H.W. Kugel, et al., Phys. Rev. 165 (1968) 1352–1360.
[32] R.E. McAdams, E.N. Hatch, Nucl. Phys. 82.2 (1966) 372–384.
[33] D.B. Fossan, B. Herskind, Nucl. Phys. 40 (1963) 24–33.
[34] A.W. Sunyar, Phys. Rev. 98 (1955) 653–657.
[35] M. Hellstrom, et al., Phys. Rev. C43 (1991) 1462–1465.
[36] M.J. Martin, Nucl. Data Sheets 114.11 (2013) 1497–1847.
[37] H. Mach, et al., Nucl. Instrum. Meth. A (1989) 49–72.
[38] E. Bodenstedt, et al., Nucl. Phys. 11 (1959) 584–598.
[39] W. Flauger, H. Schneider, Atomkernenergie 8 (1963) 453.
[40] D. Bloess, et al., Z. Phys. 192 (1966) 358.
[41] B. Olsen, L. Bostrom, Nucl. Instrum. Methods 44 (1966) 65.
[42] F.W. Richter, J. Schutt, Z. Phys. 199 (1967) 422.
[43] F.A. Akilov, et al., Izv. Akad. Nauk SSSR Ser.Fiz. 32 (1968) 808.
[44] A. Sakata, et al., Himeji Kogyo Daigaku Kenkyu Hokoku No.22A (1969) 1.
[45] K.G. Valivaara, et al., Phys. Scr. 2 (1970) 19.
[46] P.D. Bond, et al., Nuclear Phys. A 163.2 (1971) 571–576.
[47] D.K. Gupta, G. Rao, Nuclear Phys. A 182.3 (1972) 1669–1672.
[48] D. Mouchel, H.H. Hansen, Int. J. Appl. Radiat. Isot. 34.8 (1991) 1201–1210.
[49] R.L. Graham, R.E. Bell, Can. J. Phys. 31.3 (1953) 377–392.
[50] P. Thieberger, Arkiv Fysik 22 (1962) 127.
[51] J.S. Geiger, et al., Nucl. Phys. 68.2 (1965) 3352–3368.
[52] I.M. Govil, et al., Nucl. Phys. 45 (1963) 60–64.
[53] Y. Khazov, Nucl. Data Sheets 112.4 (2011) 855–1113.
[54] G.J. Wozniak, et al., Nucl. Instrum. Methods 180 (1981) 509–510.
[55] E. Lamprou, et al., Characterization of TOF-petdetectors based on monolithic blocks and ASIC-readout, 2018, arxiv preprint arXiv:1806.08715.
[56] J. Du, IEEE Trans. Radiat. Plasma Med. Sci. 1 (5) (2017) 385–390, http://dx.doi.org/10.1109/TRPMS.2017.2726534.
[57] J.M. Régis, et al., Nucl. Instrum. Methods A 684 (2012) 36.
[58] J.M. Régis, et al., Nucl. Instrum. Methods A 622 (2010) 83–92.
[59] F. Azaiez, R. Nchodu, R. Nemutudi, M. Wiedeking, Nucl. Phys. News 30 (4) (2020) 5–11, http://dx.doi.org/10.1080/10619127.2020.1832807.
[60] J.M. Régis, Fast Timing with $LaBr_3$(Ce) Scintillators and the Mirror Symmetric Centroid Difference Method (Ph.D. thesis), Köln, 2011.
[61] H. Mach, et al., Nuclear Phys. A523 (1991) 197.
[62] E.R. Gamba, A.M. Bruce, M. Rudigier, Nucl. Instrum. Meth. A928 (2019) 93–103.
[63] J. Régis, et al., Nucl. Instrum. Methods A 955 (2020) 163258, http://dx.doi.org/10.1016/j.nima.2019.163258, URL http://www.sciencedirect.com/science/article/pii/S016890021931527X.
[64] G.D. Dracoulis, J.L. Durell, W. Gelletly, J. Phys. A: Math. Nucl. Gen. 6 (11) (1973) 1772–1799, http://dx.doi.org/10.1088/0305-4470/6/11/014.
[65] G.D. Dracoulis, G.S. Foote, M.G. Slocombe, The g-factor of the 235 keV state in44sc, J. Phys. A: Math. Nucl. Gen. 7 (18) (1974) 2289–2294, http://dx.doi.org/10.1088/0305-4470/7/18/009.
[66] J.J. Kolata, et al., Phys. Rev. C 10 (1974) 1663.
[67] A.R. Poletti, et al., Phys. Rev. C 13 (1976) 1180–1193, http://dx.doi.org/10.1103/PhysRevC.13.1180, URL https://link.aps.org/doi/10.1103/PhysRevC.13.1180.
[68] M. Marmor, S. Cochavi, D.B. Fossan, Phys. Rev. Lett. 25 (1970) 1033–1035, http://dx.doi.org/10.1103/PhysRevLett.25.1033, URL https://link.aps.org/doi/10.1103/PhysRevLett.25.1033.
[69] R. Hartmann, K.P. Lieb, H. Röpke, Nuclear Phys. A 123 (2) (1969) 437–448, http://dx.doi.org/10.1016/0375-9474(69)90512-0, URL http://www.sciencedirect.com/science/article/pii/0375947469905120.
[70] R. Hartmann, H. Grawe, Nuclear Phys. A 164 (1) (1971) 209–218, http://dx.doi.org/10.1016/0375-9474(71)90851-7, URL http://www.sciencedirect.com/science/article/pii/0375947471908517.
[71] T. Nomura, C. Gil, H. Saito, T. Yamazaki, M. Ishihara, E2 Effective charges of the $f_{\frac{7}{2}}$ proton and neutron deduced from the lifetimes of the 6^+ states in ^{50}Ti, ^{54}Fe, and ^{42}Ca, Phys. Rev. Lett. 25 (1970) 1342–1345, http://dx.doi.org/10.1103/PhysRevLett.25.1342, URL https://link.aps.org/doi/10.1103/PhysRevLett.25.1342.
[72] P.M. Lewis, A.R. Poletti, M.J. Savage, C.L. Woods, The mean life of the second 0+ state in ^{42}Ca, Nuclear Phys. A 443 (2) (1985) 210–216, http://dx.doi.org/10.1016/0375-9474(85)90260-X, URL http://www.sciencedirect.com/science/article/pii/037594748590260X.
[73] P.C. Simms, N. Benczer-Koller, C.S. Wu, New application of delayed coincidence techniques for measuring lifetimes of excited nuclear states—^{42}Ca and ^{47}Sc, Phys. Rev. 121 (1961) 1169–1174, http://dx.doi.org/10.1103/PhysRev.121.1169, URL https://link.aps.org/doi/10.1103/PhysRev.121.1169.
[74] D. Bloess, F. Munnich, Untersuchung der Lebensdauer Angeregter Kernniveaus von ^{42}Ca, Z. Naturforsch. 18 (1963) 671.